Supplementary Information (SI) for Physical Chemistry Chemical Physics.

SUPPORTING INFORMATION

Tuneable stimuli-responsive behaviour, spectroscopic signatures and redox properties of indolo[3,2-b]carbazole-based diradicals

Irene Badía-Domínguez, [a] Deliang Wang,[b] Rosie Nash,[c] Víctor Hernández Jolín,[a] David Collison,[d] Muralidharan Shanmugam,[d] Hongxiang Li,[b,e]* František Hartl, [c]*, M. Carmen Ruiz Delgado [a]*

[a] Department of Physical Chemistry, University of Málaga, Campus de Teatinos s/n, 229071, Málaga, Spain. E-mail: carmenrd@uma.es

[b] Key Laboratory of Synthetic and Self-assembly Chemistry for Organic Functional Materials, Shanghai Institute of Organic Chemistry, Chinese Academy of Sciences, Shanghai, 200032, China.

[c] Department of Chemistry, University of Reading, Whiteknights, Reading RG6 6DX, United Kingdom. E-mail: f.hartl@reading.ac.uk

[d] Photon Science Institute and Department of Chemistry, The University of Manchester, Manchester M13 9PL, United Kingdom.

[e] Key Laboratory for Advanced Materials, Feringa Nobel Prize Scientist Joint Research Center, Frontiers Science Center for Materiobiology and Dynamic Chemistry, Institute of Fine Chemicals, School of Chemistry and Molecular Engineering, East China University of Science and Technology, Shanghai, 200237, China. Email: lihongxiang@ecust.edu.cn

Table of contents:

1. Syntheses

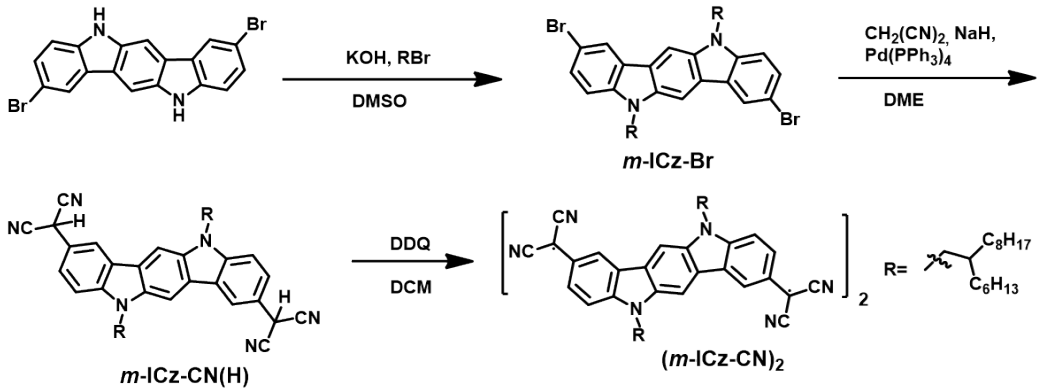

Scheme S1. The synthetic path to ***m*-ICz-Br** and (***m*-ICz-CN**)$_2$.

Synthesis of *m*-ICz-Br

A mixture of 2,8-dibromo-5,11-dihydroindolo[3,2-b]carbazole (1.900 g, 4.59 mmol), tetrabutylammonium iodide (0.163 g, 0.44 mmol) and 2-hexyl-1-decyl bromide (3.984 g, 13.05 mmol) in DMSO (25 mL) and THF (10 mL) were added into a 50-mL flask. A freshly prepared 50% aq. NaOH solution (2 mL) was dropped into the solution, and the mixture was stirred at room temperature for 1 h and then at 70 °C for 8 h. After cooling to the room temperature, the mixture was poured into water (60 mL). The organic material was extracted with petroleum ether (30 mL × 3). The combined organic was washed with water (50 mL × 3) and brine (50 mL) and then dried over anhydrous $MgSO_4$. After evaporating the solvent under vacuum, the residue was purified by column chromatography on silica gel (hexane) to give a yellow oil that turned to yellow solid **3** (1.878 g, 47.4 %). ^{1}H NMR (300 MHz, $CDCl_3$) δ 0.85 (t, *J* = 7.3 Hz, 12H) , 1.50 – 0.99 (m, 48H) , 2.19 (s, 2H) , 4.19 (s, 4H) , 7.26 (s, 2H) , 7.54 (d, *J* = 8.0 Hz, 2H) , 7.89 (s, 2H), 8.26 (s, 2H); MS (MALDI-TOF) *m/z*: 862.2 $[M]^+$; HRMS (MALDI) *m/z*: calcd for $C_{50}H_{74}N_2Br_2^+$ 860.4213, found 860.4190.

Synthesis of *m*-ICz-CN(H)

Malononitrile (0.391 mg, 5.92 mmol) was added to an ice-water-cooled suspension of sodium hydride (0.288 mg, 12.0 mmol) in 1,2-dimethoxyethane (15 mL) under a nitrogen stream. The mixture was stirred at room temperature for another 30 min. Then ***m*-ICz-Br** (0.513 g, 0.594 mmol) and tetrakis(triphenylphosphine)palladium (71 mg, 0.061 mmol) were added, and the solution was heated at 100 °C for 12 h. The resulting solution was quenched with water carefully and extracted with CH_2Cl_2. After drying over $MgSO_4$, the solvent was removed by rotary evaporation and the crude

product was purified by silica gel column chromatography (eluent: petroleum ether/CH_2Cl_2 = 3:1, v/v) to yield ***m*-ICz-CN(H)** (0.201 g, 40.8%).^{1}H NMR (400 MHz, CD_2Cl_2) δ 0.82 (q, *J* = 6.9 Hz, 12H)， 1.20 (m, 48H), 2.27 (m, 2H), 4.33 (d, *J* = 7.6 Hz, 4H), 5.36 (s, 2H), 7.53 (d, *J* = 8.5 Hz, 2H), 7.57 (dd, *J* = 8.6, 1.9 Hz, 2H), 8.36 (d, *J* = 1.5 Hz, 2H). MS (MALDI-TOF) *m/z*: 832.6 $[M]^+$; HRMS (MALDI) *m/z*: calcd for $C_{56}H_{76}N_6^+$ 832.6126, found 832.6122.

Synthesis of (*m*-ICz-CN)$_2$

To the mixture of ***m*-ICz-CN(H)** (0.202 g, 0.242 mmol) in CH_2Cl_2 (15 mL) was added a solution of 2,3-dichloro-5,6-dicyano-1,4-benzoquinone (DDQ) (78 mg, 0.343 mmol) in CH_2Cl_2 (5 mL). After stirring for 20 minutes, the mixture was filtered. Methanol (10 mL) was added to the filtrate and then most of the solvent was removed by rotary evaporation so as to precipitate a solid. The solid was filtered and dried, affording **(*m*-ICz-CN)$_2$** (0.157 g, 78.0%). ^{1}H NMR (300 MHz, $CDCl_3$) δ 0.86 – 0.69 (m, 12H) , 1.15 (m, 48H) , 2.00 (br, 2H) , 3.97 (m, 2H) , 4.32 (m, 2H) , 6.24 (s, 2H) , 6.52 (s, 2H) , 7.61 (d, *J* = 8.7 Hz, 2H), 8.02 (d, *J* = 8.5 Hz, 2H); ^{13}C NMR (101 MHz, $CDCl_3$) δ 143.27, 143.26, 136.77, 136.75, 124.95, 122.59, 122.04, 121.99, 113.27, 111.64, 111.05, 109.24, 97.69, 54.09, 48.44, 37.85, 37.83, 31.93, 31.84, 31.79, 31.72, 30.05, 29.75, 29.71, 29.61, 29.49, 29.39, 29.35, 29.19, 26.88, 26.85, 26.62, 26.57, 22.73, 22.68, 22.62, 22.51, 14.17, 14.13, 14.09, 14.00. MS (MALDI-TOF) m/z: 830.5 $(M)^+$; HRMS (MALDI) *m/z*: calcd for $C_{56}H_{74}N_6^+$ 830.5970, found 830.5947 Anal. Calcd for $C_{56}H_{74}N_6$: C, 80.92; H, 8.97; N, 10.11; Found: C, 80.61; H, 8.99; N, 9.98.

2. Complementary techniques

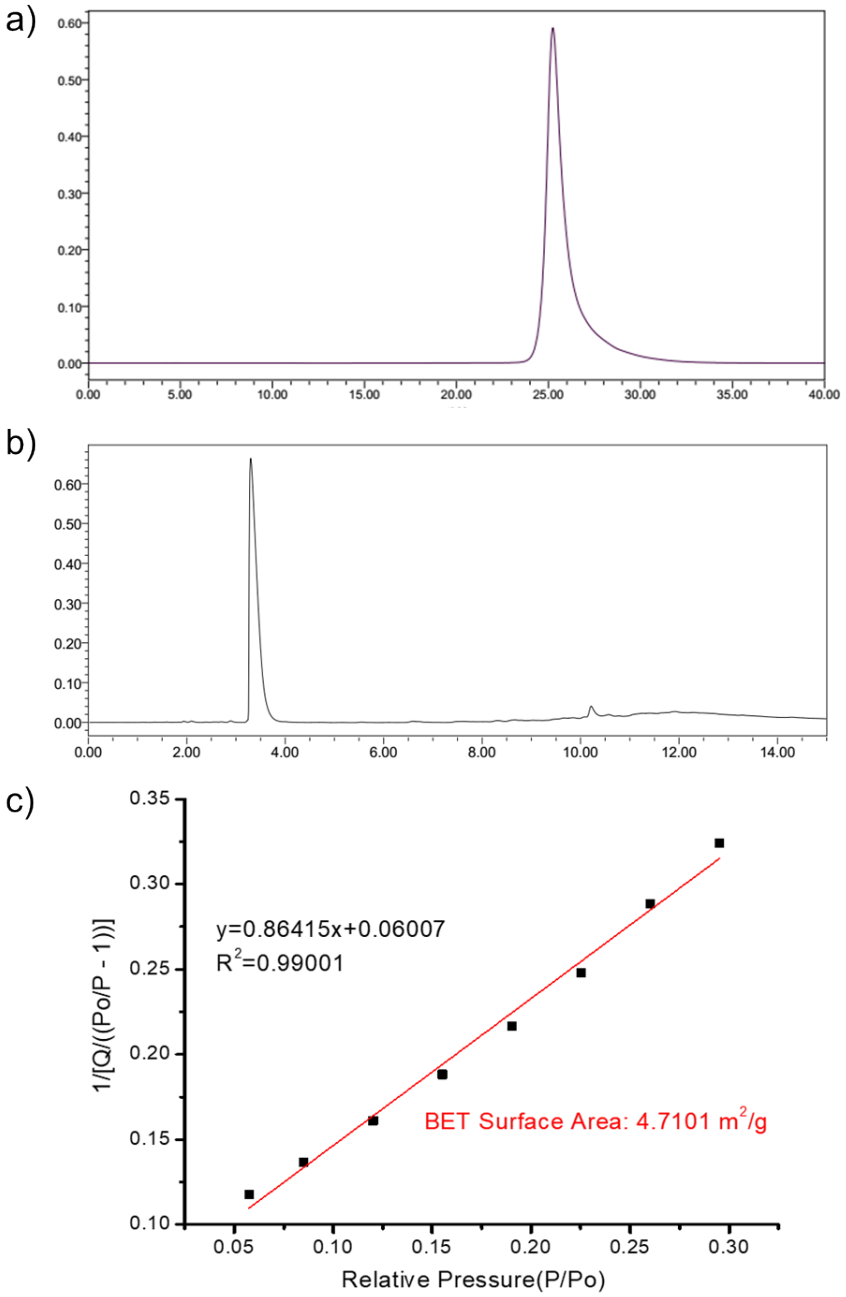

Figure S1. (a) GPC elution curve of **(*m*-ICz-CN)$_2$**. (b) HPLC elution curve of **(*m*-ICz-CN)$_2$** in solution at room temperature. (c) The Brunauer-Emmett-Teller (BET) surface area plot **(*m*-ICz-CN)$_2$** was calculated from the nitrogen adsorption-desorption isotherm.

3. NMR spectroscopy

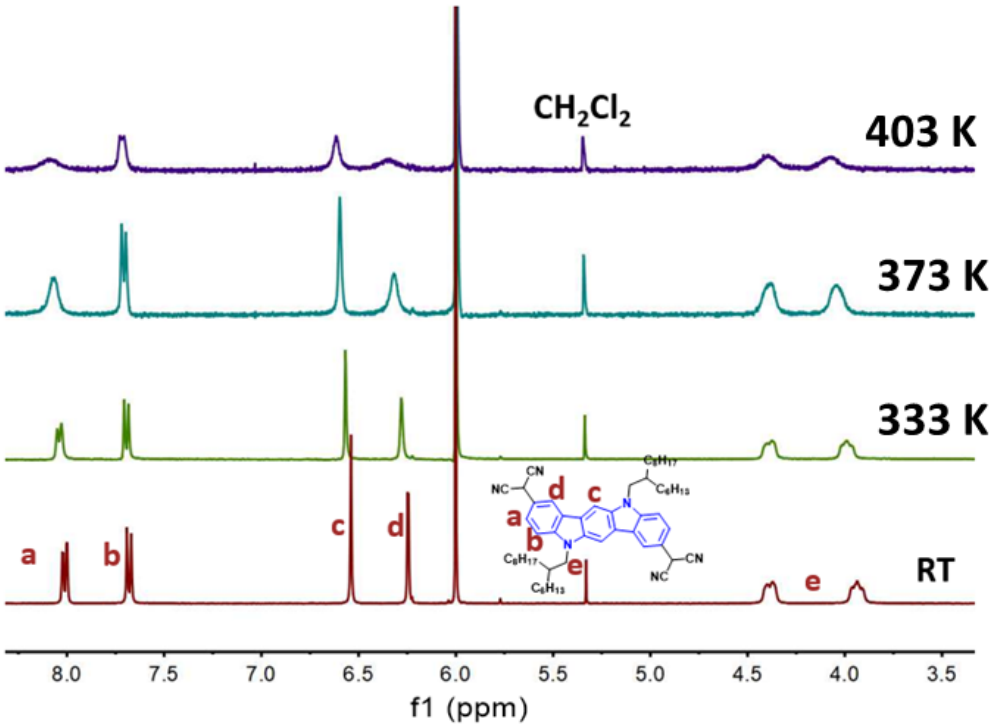

Figure S2. Variable-temperature ^{1}H NMR spectra of **(*m*-ICz-CN)$_2$** in tetrachloroethane-d_2.

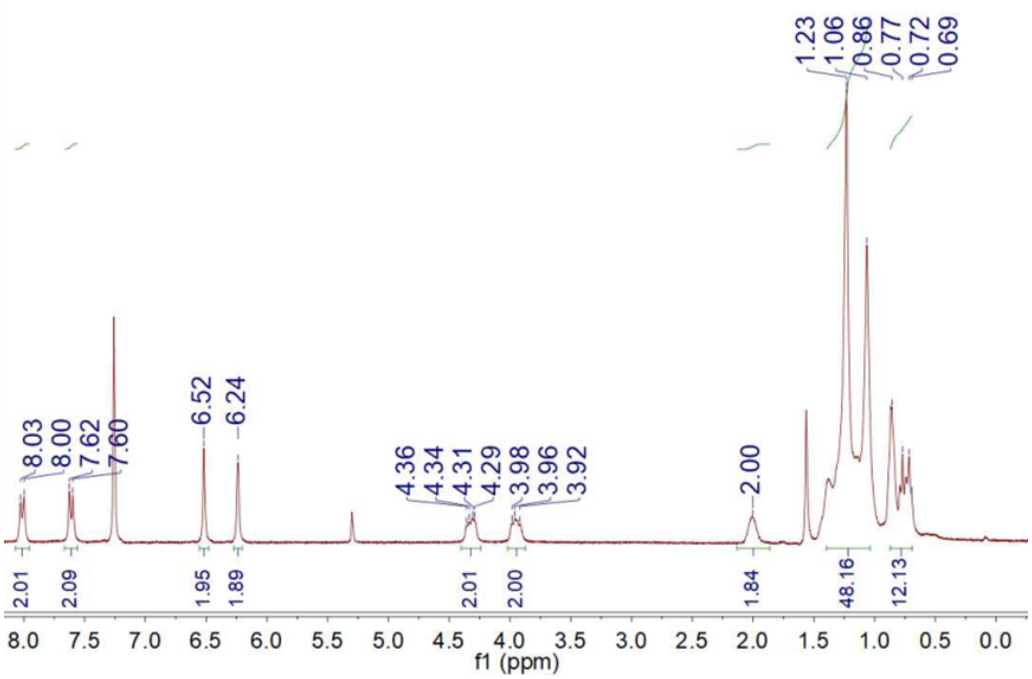

Figure S3. ^{1}H NMR spectrum of **(*m*-ICz-CN)$_2$** in chloroform-d_1 at RT.

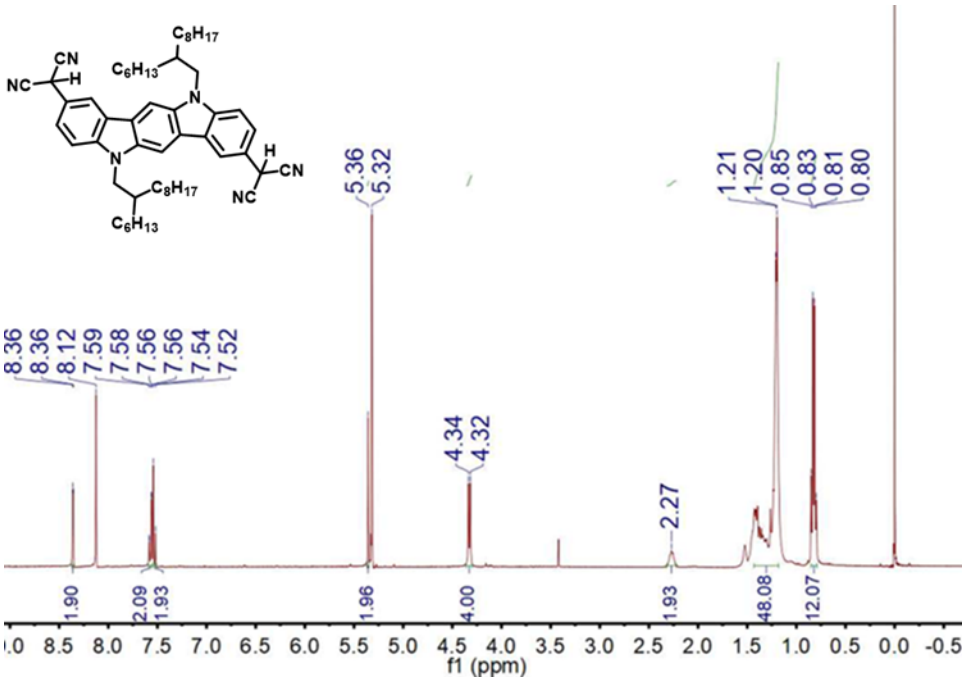

Figure S4. ^{1}H NMR spectrum of precursor ***m*-ICz-CN(H)** in dichloromethane-d_2 at RT.

4. Mass spectroscopy

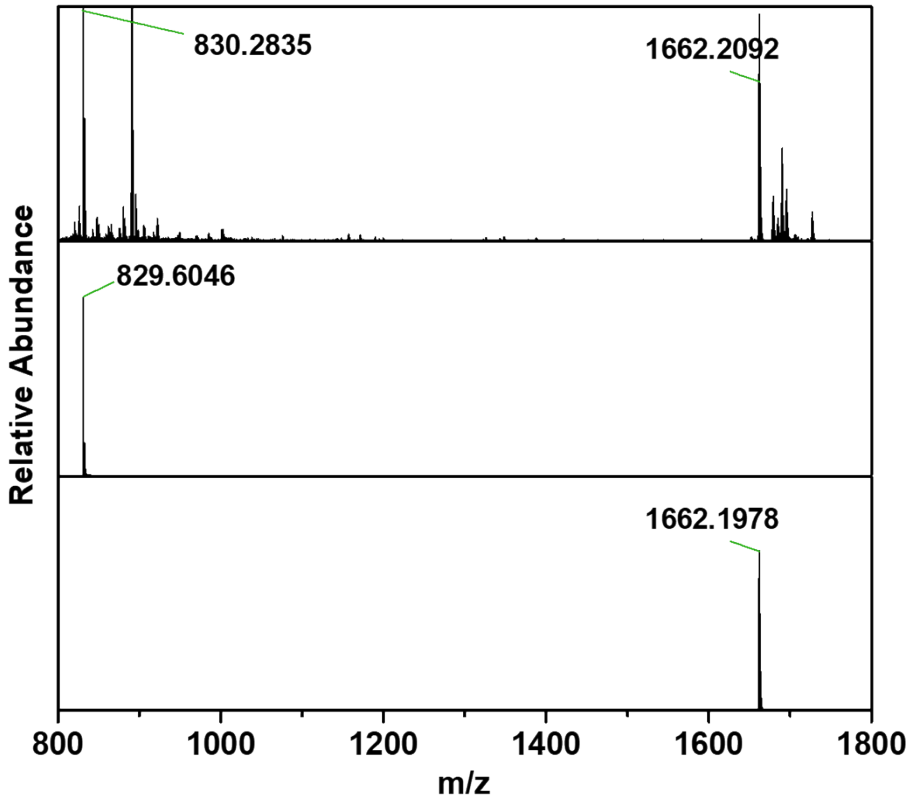

Figure S5. Theoretical mass spectra of monomer ***m*-ICz-CN(H)** (middle) and dimer cyclophane **(*m*-ICz-CN)$_2$** (bottom), and the experimental ESI-MS spectrum of **(*m*-ICz-CN)$_2$** (top) showing also the presence of ***m*-ICz-CN**. Assignment of the *m/z* values: calc. 829.60 and exp. 830.28 for ***m*-ICz-CN** (M^+); calc.1662.20 and exp. 1662.21 for **(*m*-ICz-CN)$_2$** (M_2^{2+}).

5. DFT calculations

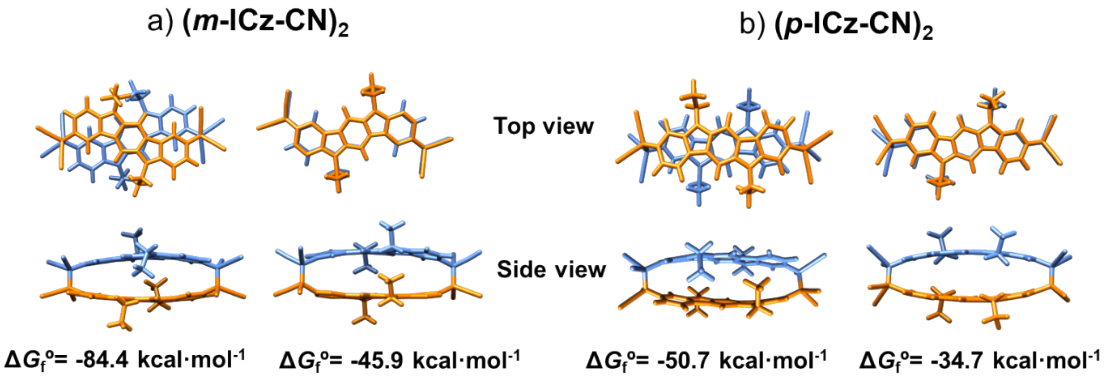

Figure S6**.** DFT-calculated global minima structures for antiparallel (left) and parallel (right) conformations of (a) **(*m*-ICz-CN)$_2$** and (b) **(*p*-ICz-CN)$_2$**. The values of the Gibbs free energy of formation (at 298 K) are also presented.

Table S1. DFT-calculated relative energies and summarized physical properties of ***p*-ICz-CN** and ***m*-ICz-CN** compounds at (U)M06-2X/6-31G**.

Molecules	$\Delta E_{OS\text{-}CS}$ (kcal·mol^{-1})	$\Delta E_{S\text{-}T}$ (kcal·mol^{-1})	J_{ab} (kcal·mol^{-1})	HL gap (eV)	*S**2*	
					OS	T
***p*-ICz-CN**	-10.92	-3.26	-1.59	2.28	1.01	2.04
***m*-ICz-CN**	-24.27	-0.37	-0.18	1.21	1.04	2.04

Table S2. Free energy of formation values (at 298 K) calculated by the PCM method at the M06-2X/6-31G** level of **(*p*-ICz-CN)$_2$** and **(*m*-ICz-CN)$_2$** in toluene, chloroform, *o*-dichlorobenzene.

Compound	ΔG_f^0 (kcal·mol^{-1})			
	Gas-phase	Toluene (ε = 2.4)[a]	Chloroform (ε = 4.7)[a]	*o*-dichlorobenzene (ε = 9.9)[a]
(*p*-ICz-CN)$_2$	–50.7	–42.6	–38.9	–37.0
(*m*-ICz-CN)$_2$	–84.4	–60.1	–55.0	–51.2

[a] Dielectric constant.

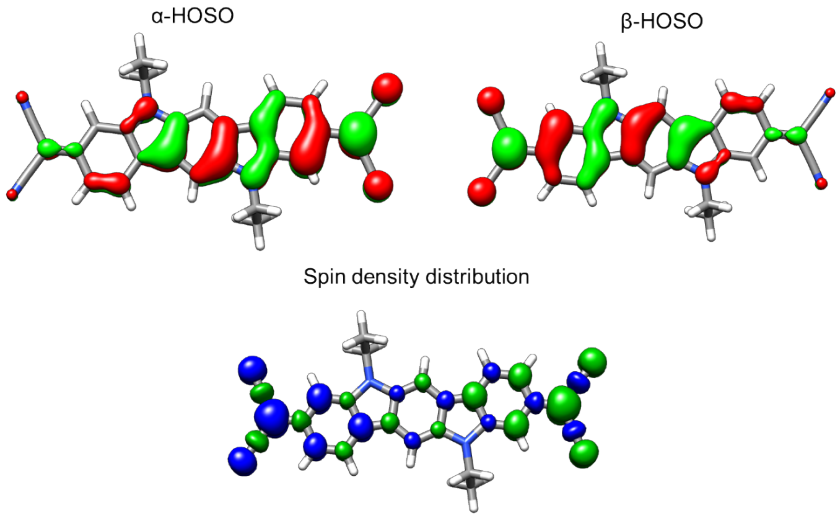

Figure S7. DFT-calculated highest-occupied single orbitals (HOSO) of the α and β electrons (top) together with the spin density distribution in the diradical singlet ground state of ***p*-ICz-CN** at the (U)M06-2X/6-31G** level of theory with an isosurface value of 0.03 a.u. The blue and green surfaces represent α and β spin densities, respectively.

6. Optical properties and TD-DFT calculations

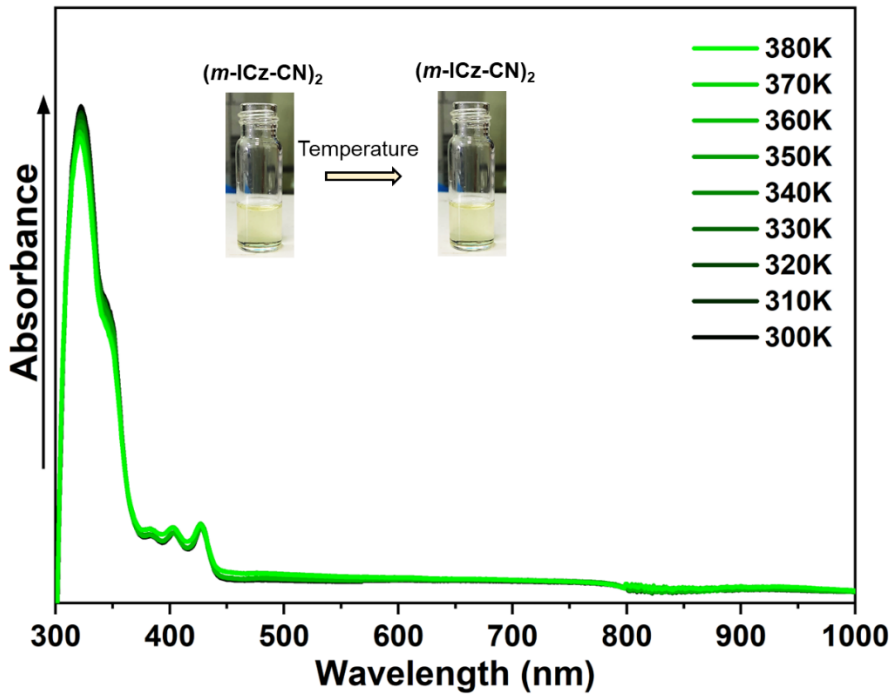

Figure S8. UV-Vis-NIR absorption of **(*m*-ICz-CN)$_2$** in toluene.

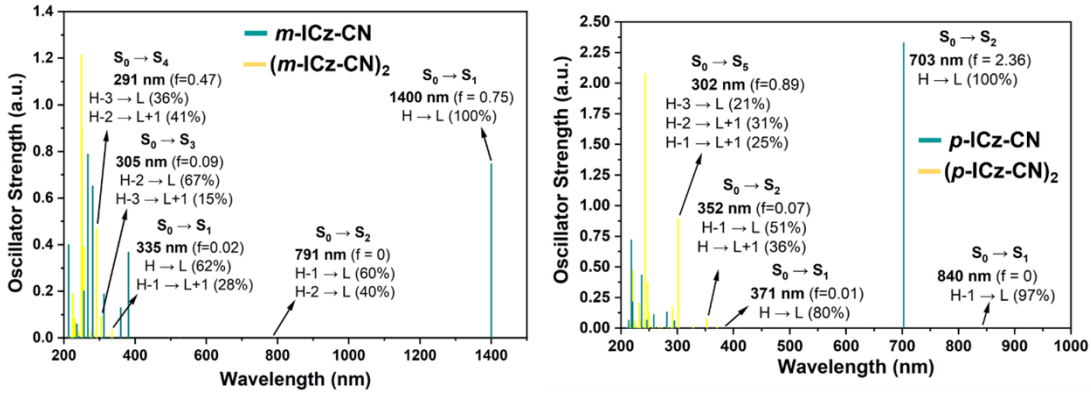

Figure S9. TD-DFT calculated vertical transition energies for **(*m*-ICz-CN)$_2$** (left) and **(*p*-ICz-CN)$_2$** (right) dimer cyclophanes (yellow vertical lines) and CS singlet diradical (green vertical lines) at ωB97XD/6-31G** //M06-2X/6-31G** level of theory.

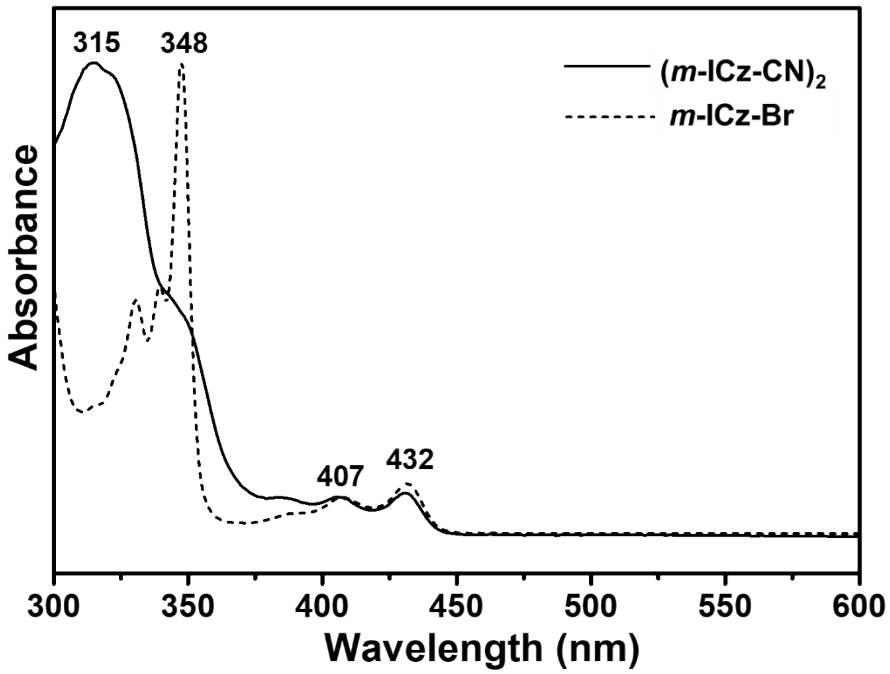

Figure S10. Experimental UV-Vis absorption spectra of **(*m*-ICz-CN)$_2$** (solid line) and ***m*-ICz-Br** (dashed line) in dichloromethane at ambient temperature.

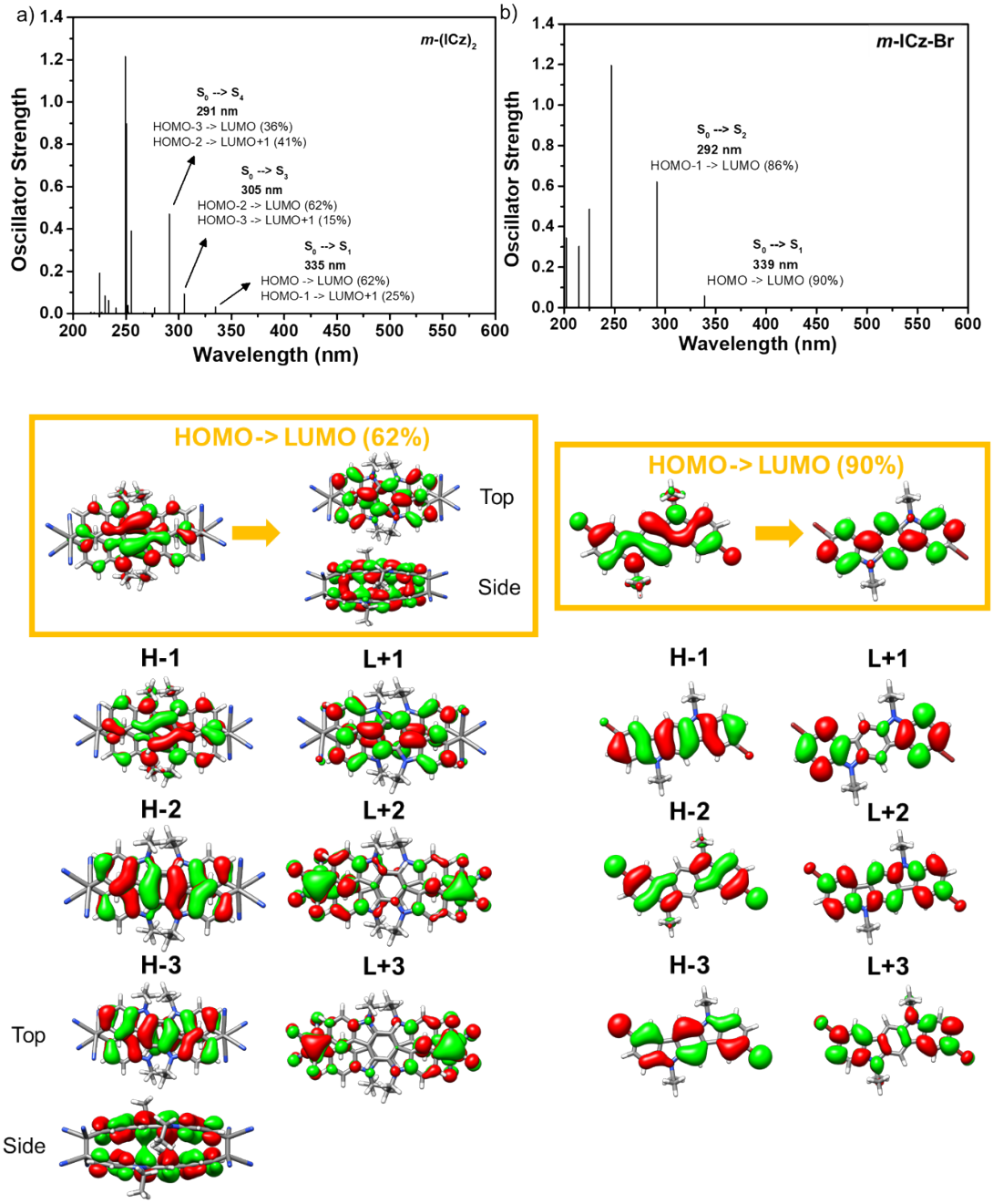

Figure S11. Theoretical absorption spectra of **(*m*-ICz-CN)$_2$** (a) and its brominated precursor ***m*-ICz-Br** (b) in Scheme S1, together with the electronic excitations (wavelength vs. oscillator strength) shown as vertical bars, by using TD-DFT at ωB97XD/6-31G**//M06-2X/6-31G** level of theory. The isosurface plots (isovalue 0.02 a.u.) of the frontier molecular orbitals are also shown.

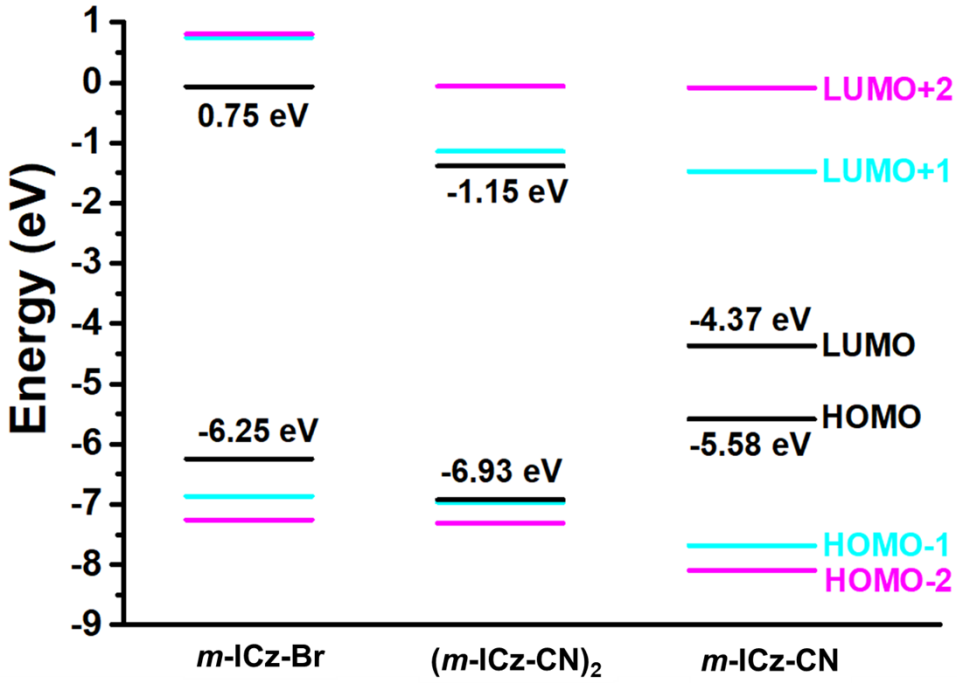

Figure S12. Diagram of the frontier molecular orbital energies corresponding to precursor ***m*-ICz-Br**, dimer cyclophane **(*m*-ICz-CN)$_2$** and closed-shell monomer ***m*-ICz-CN**, calculated at the M06-2X/6-31G** level.

7. Redox properties

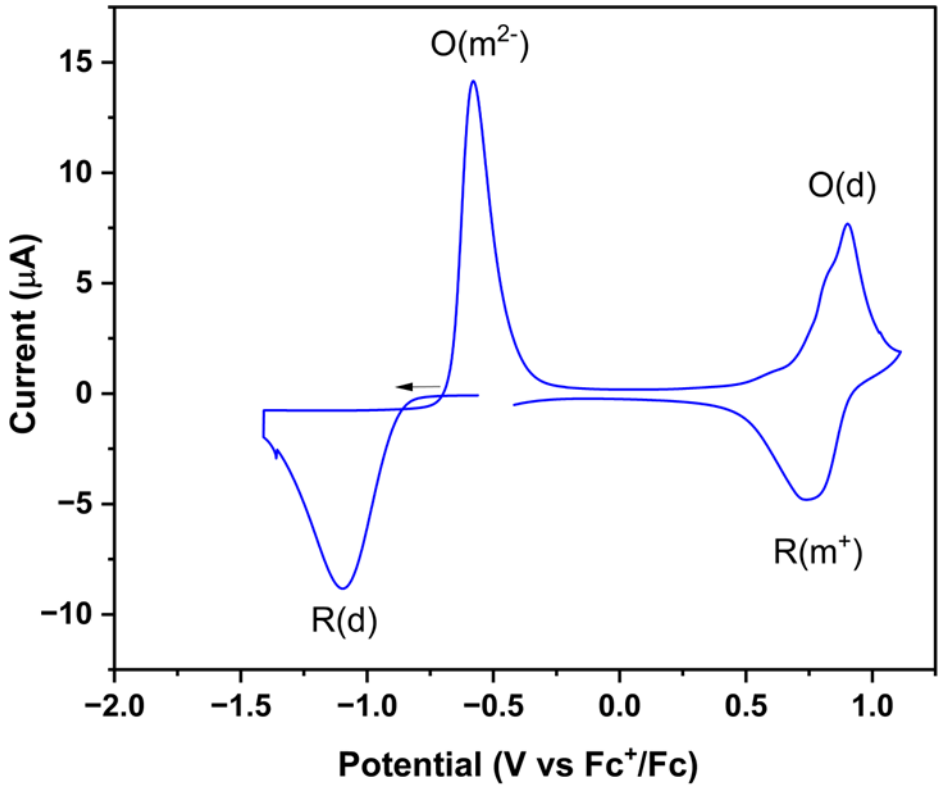

Figure S13. Thin-layer cyclic voltammogram of **(*m*-ICz-CN)$_2$** in CH_2Cl_2 at T = 293 K; v = 2 mV s^{-1}, Pt minigrid in an OTTLE cell.

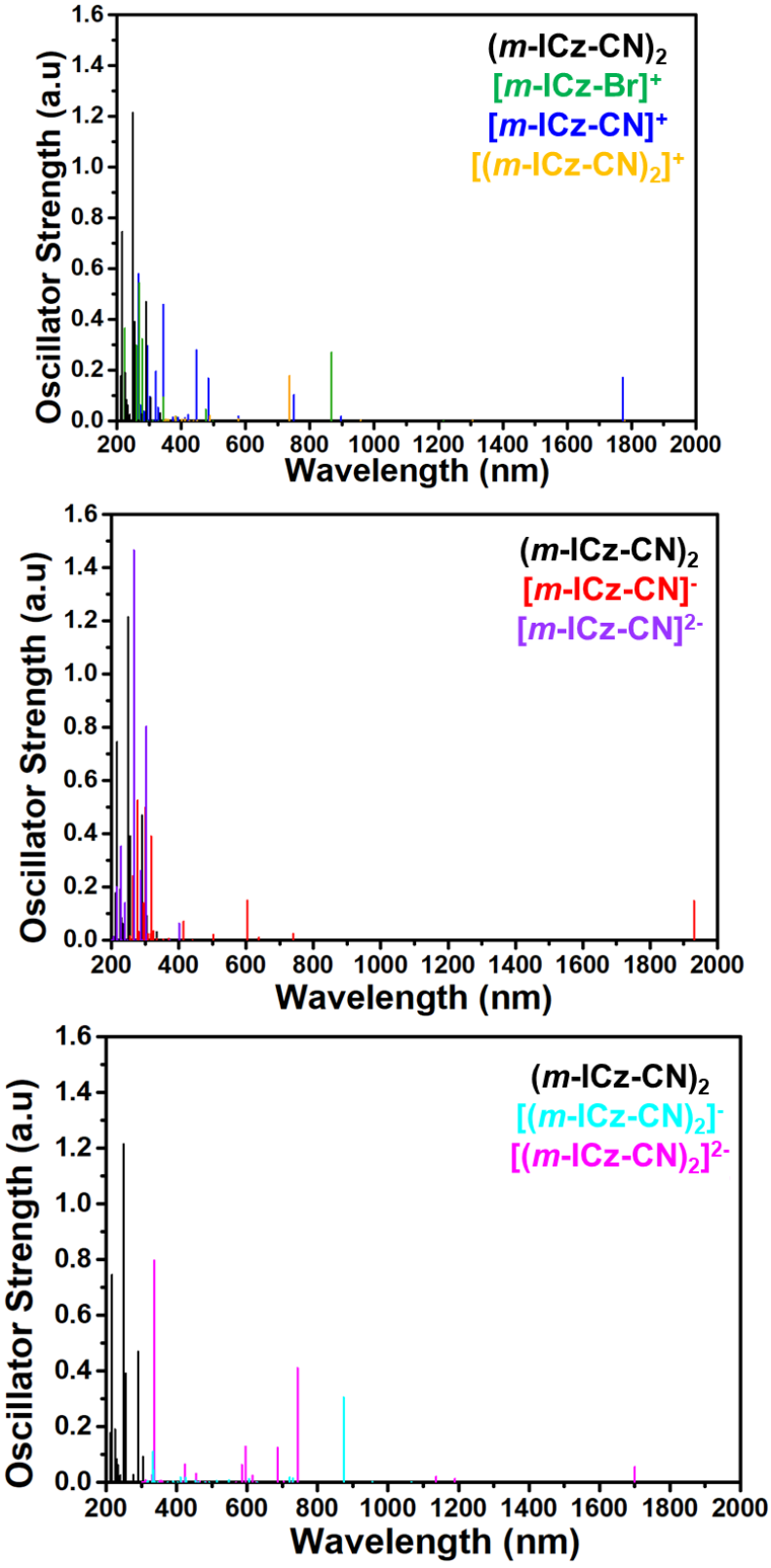

Figure S14. TD-DFT-calculated (at the (U)ωB97XD/6-31G**//M06-2X/6-31G** level of theory) vertical transition energies for cyclophane dimer radical cation [(***m***-ICz-CN)$_2$]$^+$, monomer cation [***m***-ICz-CN]$^+$ and reference radical cation [***m***-ICz-Br]$^+$ (top), monomer radical anion [***m***-ICz-CN]$^-$ and dianion [***m***-ICz-CN]$^{2-}$ (middle), and cyclophane dimer radical anion [(***m***-ICz-CN)$_2$]$^-$ and dianion [(***m***-ICz-CN)$_2$]$^{2-}$ (bottom).

Table S3. Calculated (TD-DFT, at the ωB97XD/6-31G**//M06-2X/6-31G** level of theory) and reference experimental (in dichloromethane) electronic absorption maxima for neutral σ-dimer **(*m*-ICz-CN)$_2$**, isolated monomer ***m*-ICz-CN,** reference ***m*-ICz-Br,** and their different redox states.

Compound		λ_{exp} (nm)	λ_{calc} (nm)
Neutral	**(*m*-ICz-CN)$_2$**	432/407, 344sh, 315, 290	335, 305, 291, 249
	***m*-ICz-Br**	410, 348, 292	339, 292, 247
	***m*-ICz-CN**	888,707,615,432,407	1400,791 381, 281
Radical Cation	[**(*m*-ICz-CN)$_2$**]$^+$	---	737, 490, 381
	[***m*-ICz-Br**]$^+$	<1000, 899sh 541, 426, 325	868, 476, 344, 306
	[***m*-ICz-CN**]$^+$	953, 807 500-400(sh) 380, 362, 333	1773, 751, 484, 447, 345
Radical Anion	[**(*m*-ICz-CN)$_2$**]$^-$	---	874, 721, 606, 411, 334
	[***m*-ICz-CN**]$^-$	---	1931, 604, 415, 318
Dianion	[**(*m*-ICz-CN)$_2$**]$^{2-}$	---	743, 686, 596, 337
	[***m*-ICz-CN**]$^{2-}$	495/465, 370/352, 316/303	401, 303/287, 267

8. Raman spectroscopy

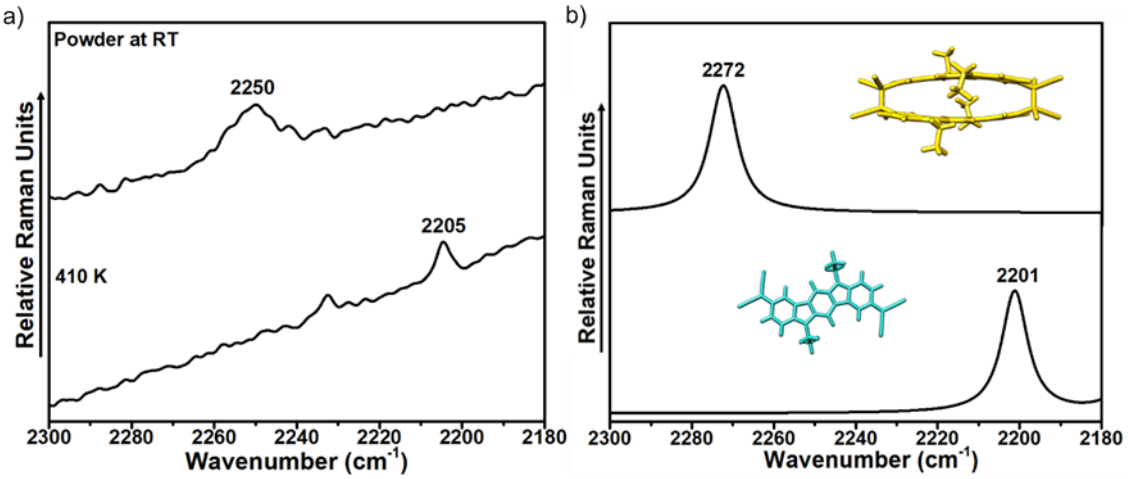

Figure S15. (a) Top: FT-Raman spectra of the solid yellow powder of **(*m*-ICz-CN)$_2$** at the 1064-nm laser line. Down: Raman spectrum of isolated diradical ***m*-ICz-CN** in the solid state at 410 K at the 785-nm laser line. (b) Theoretical Raman spectra of **(*m*-ICz-CN)$_2$** (top) and ***m*-ICz-CN** (down) at the M06-2X/6-31G** level.

9. EPR spectroscopy

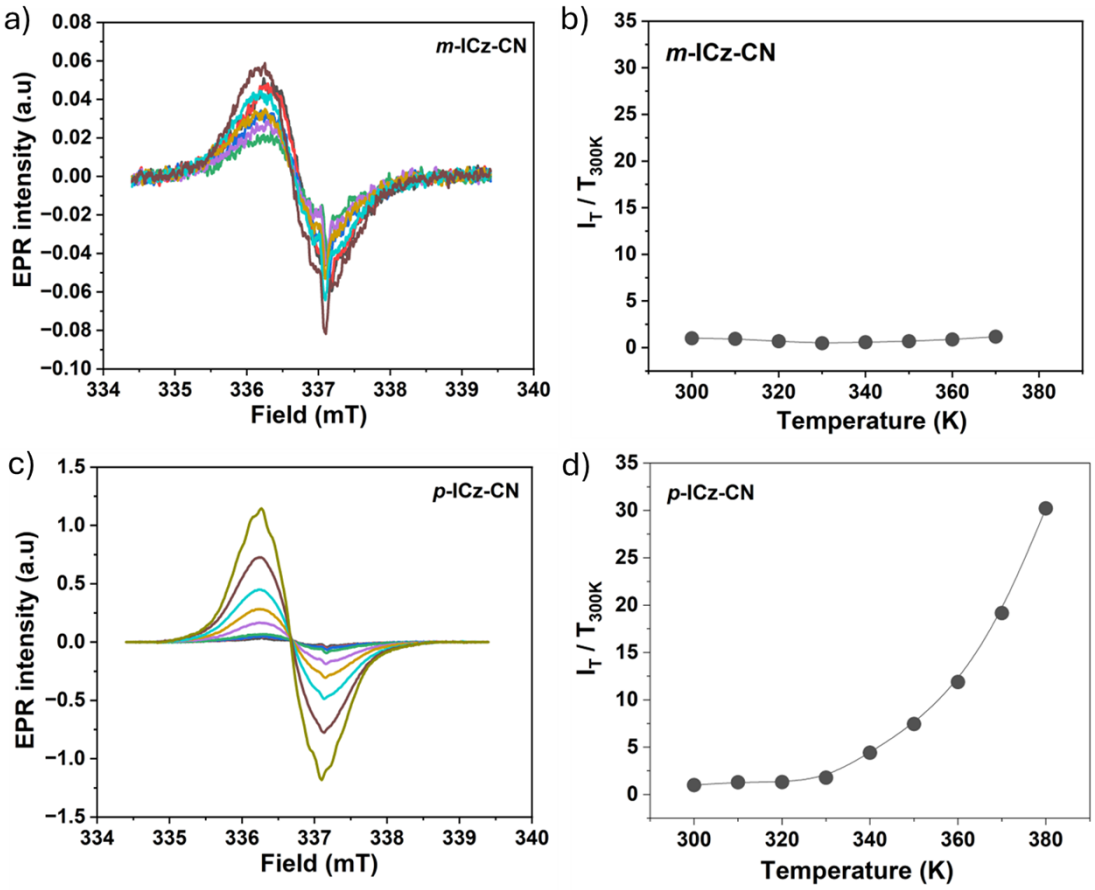

Figure S16. Variable Temperature, cw-EPR spectra of diradical (a) ***m*-ICz-CN** and (c) ***p*-ICz-CN** generated from dimer cyclophane **(*m*-ICz-CN)$_2$** and **(*p*-ICz-CN)$_2$,** respectively, in toluene upon gradual temperature elevation from 300 K to 380 K. Experimental Conditions: as provided under methodology section "EPR Spectroscopy" and in Figure 6 main-text. *T*-dependent relative intensities of EPR signals of diradicals (b) ***m*-ICz-CN** and (d) ***p*-ICz-CN** measured as fluid solution in toluene.

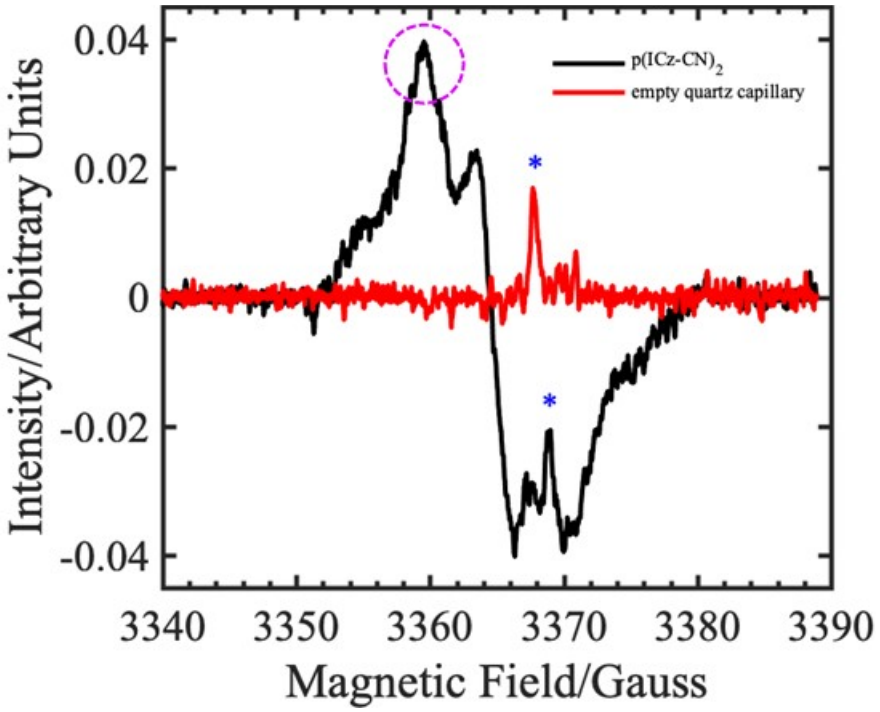

Figure S17. The EPR spectrum of the empty quartz-capillary is shown in the middle panel (red trace). The sharp EPR signal observed at 3368 G (indicated by the blue asterisk marks) is likely due to the quartz impurity; this trace signal is observed in all our EPR experiments.